Jurnal Tribologi 42 (2024) 129-145

MYTRIBOS Malaysian Tribology Society

Jurnal Tribologi

Website : jurnaltribologi.mytribos.org e-issn: 2289-7232

# Tribological properties of the multilayer thin films deposited on the free-form shaped Ti13Nb13Zr alloy

Ali Kemal Aslan [1*], Erkan Bahçe [2]

[1] Department of Metal and Machinery Technologies, Tunceli Vocational School, Munzur University, TURKEY.
[2] Department of Mechanical Engineering, İnonu University, TURKEY.
[*]Corresponding author: akaslan@munzur.edu.tr

KEYWORDS

Free-form surface
Multilayer coating
Biomaterial
Thin films
Wear

ABSTRACT

Surface coating processes are carried out to increase the wear and corrosion resistance of products with free-form surfaces used in the biomedical field. In this study, Ti/TiN/TiC/TiCN/TaN multilayer thin films were deposited on the surface of Ti13Nb13Zr alloy samples with different radii of curvature using the closed-field unbalanced magnetron sputtering technique. The wear and adhesion properties of thin films were examined with a specially developed wear test setup, in a simulated body fluid environment and an ultra-high molecular weight polyethylene (UHMWPE) counterpart was used. Scanning electron microscope and X-ray diffraction measurements were used to study the morphology and microstructure of the thin films before and after wear experiments. The delamination amounts of the coatings on the sample surfaces after the wear test were measured and this value was calculated as 8.73%, 12.16%, and 16.89% for the R14, R18, and R22 samples, respectively. As a result of these findings, it was determined that the wear resistance of the coatings decreased as the radius of the curvature increased. The wear amounts of the UHMWPE components are found as 15.45, 6.75, 8.15, 15.45, 6.75, and 8.15 mg for P0, P14, P18, and P22 samples, respectively.

Received 28 November 2023; received in revised form 21 February 2024; accepted 5 June 2024.
To cite this article: Aslan and Bahçe (2024). Tribological properties of the multilayer thin films deposited on the free-form shaped Ti13Nb13Zr alloy. Jurnal Tribologi 42, pp.129-145.

## 1.0 INTRODUCTION

Free-form surfaces are more useful both aesthetically and functionally compared to flat surfaces. Therefore, in many industries such as optics, astronomy, automotive, aerospace, and biomedical fields free-form shaped products are preferred (Buyong et. al, 1998; Ye et al., 2017; Miura et al., 2014; Bahçe et al., 2020; Gong et al., 2023). Especially, implants that replace hard tissue used in biomedical applications have free-form surfaces. The release of some cytotoxic elements in the compositions of implant materials used in this field to tissues and body fluids causes infections and reduces the lifetime of the implant (Lützner et al., 2013; Skjöldebrand et al., 2013; Hussein et al., 2023). To overcome this problem, metallic implant materials are coated with mono or multilayer ceramic thin films such as TiN, ZrN (Kumar et al., 2021). Although the lifetime of the implants has been increased with these coatings, it has been reported in previous studies that they fail earlier than the lifetimes evaluated in-vitro experiments (Herbster et al., 2020). One of the reasons for this situation is thought to be due to the fact that these experiments were carried out on flat surface samples. While coatings made by various methods such as PVD, CVD, electrophoretic, and atomic layer deposition are mostly in a homogeneous structure with continuity on flat surfaces, this situation changes on curved surfaces.

When the previous studies are examined, it is seen that there are very few studies on the characterization of thin film coatings on freeform surfaces. Most of these are studies in which chiral and sculptured thin films are deposited on flat surfaces (Robbie et al., 1997; Schmidt et al., 2011; Esfendiar et al., 2013; Martín-Palma et al., 2013; Abdi et al., 2015; Rahchamani et al., 2015; Savaloni et al., 2017; Savari et al., 2018; Grineviciute et al., 2020). There are a few studies on thin film coatings characterization deposited on free form surfaced substrates. Kvasnicka et al. investigated the surface continuity of the TiN coatings deposited on cutting blades that have differentiated radii between 5 μm to 200 μm. As a result, they have reported coating failure at low radius values between 5-10 μm, and in other regions, they determined that the morphology of the coating showed differences with the changing radius values (Kvasnicka et al., 1999). Structural changes of thermal protective coatings deposited on free-form shaped CSMX4Ni super alloy used in high-temperature applications were studied (Liu et al., 2013). They found that the coatings had different thicknesses in different regions of the substrate and reported that the microstructure of the coating also showed differences. In another study, Hirata et al. deposited DLC coatings on trench-shaped substrates by bipolar plasma-based ion implantation. In terms of film thickness, they measured the highest thickness value at the top of the trench and the lowest thickness at the inner wall. As a result of Raman spectrometry analysis, they determined that while the hardness results were in the same order of magnitude, the microstructural properties were the same as the Si plate at the top and top of the trench, but differed on the inner walls (Hirata et al., 2015). It is concluded that more recent studies focused on deposition of thin films on flat surfaces by glancing angle deposition method (Lopes et al., 2023; Soltane et al., 2023; Pourzadeh et al., 2023; Gao et al., 2023).

The characterization of the coatings deposited on implant materials in the biomedical field is carried out in wear simulators by the relevant ISO standards. When these studies were investigated, although the vast majority of implants had free-form surfaces, it was determined that no study examined the effect of surface curvature on the continuity and microstructure of the coating (Reyna et al., 2018; Kopova et al., 2019; Schroeder et al., 2020; Rothammer et al., 2023; Rafiq et al., 2023, Birkett et al., 2023).

Among the metallic materials used in the biomedical field, titanium alloys are preferred due to their high corrosion resistance, mechanical properties, biocompatibility, and low density (Zhang

et al., 2019). Although the Ti6Al4V alloy is the most widely used in this area, release of the V element into body fluids causes damage to the tissues and premature failure of the implant (Gomes et al., 2011; Zhang et al., 2018; Pu et al., 2023; Senopati et al., 2023). Since Ti13Nb13Zr alloy does not contain any cytotoxic elements in its composition, it is an alternative biomaterial to this alloy (Li et al., 2014; Pawłowski et al., 2023). However, its low wear and fatigue strength limits its use in hard tissue replacement (Kaur et al., 2019; Senopati et al., 2023). It is observed that most of the previous studies to improve the surface properties of the Ti13Nb13Zr alloy were to increase the osteointegration and bioactivity of the alloy (Ossowska et al., 2014; Kazek-Kesik et al., 2015; Kazek-Kesik et al., 2016; Sowa et al., 2015; Urbanczyk et al., 2016; Stroz et al., 2017; Pawłowski et al., 2023; Ibrahim et al., 2023). Except these, Piotrowska and Madej have studied the tribological properties of the silver-doped titanium nitride-coated Ti13Nb13Zr alloy and have reported that Ag-doped TiN coating provided better tribological properties (Piotrowska and Madej, 2023).

In this study, coated Ti13Nb13Zr alloy samples with different curvatures were produced, the relationship between surface curvature and coating continuity was examined, and the effects of surface form on adhesion, thickness, and wear properties of the coating were examined.

## 2.0 EXPERIMENTAL PROCEDURE

### 2.1 Design of Free-Form Surfaces

Bezier, Spline, B-Spline, and Nurbs parametric curves are used in the mathematical design of free-form surfaces (Jiang et al., 2020). Especially B-spline and Bezier curves are used in this type of design. The concept of the B-spline curve was developed to solve the inadequacies of the Bezier curve. In a Bezier curve, changing the position of any of the control points changes the form of the entire curve. But, B-spline curve is the only a specific segment of the curve-shape gets changes or affected by the changing of the corresponding location of the control points. In the B-spline curve, the control points impart local control over the curve-shape rather than the global control like Bezier-curve. A spline curve is a mathematical representation for which it is easy to build an interface that will allow a user to design and control the shape of complex curves and surfaces. In a B-Spline is a basis function that contains a set of control points. A control polygon is formed with these points, and these polygon points act like a magnet, allowing the curve to follow the shape of the polygon (Miura et al., 2014; Özdemir, 2015). The B-Spline curves are specified by Bernstein basis function that has limited flexibility. B-spline curves are defined with control points, and the generated curves do not pass through these control points except at the start and end points. Another parameter affecting the form of B-spline curves is the knot vector showing the parameter variation of the B-spline curve. The knot vectors determine how many polynomial segments the B-spline curve will consist of. The mathematical expression for a B-spline curve of k degree with (n+1) control points can be given as follows (Ayhan, 2003):

$$P(u,v)=\sum_{i=1}^{n+1} B_i N_{i,k}(t) \qquad t_{\min} \le t < t_{\max} \quad 2 \le k < n+1 \tag{1}$$

Where the;

$N_{i,k}$ : (i). base function with k. degree

$k$ : degree of the curve

$x_i$ : Elements of the knot vector

$t$ : Parameter of the curve

$n+1$ : presents the number of the control points.

$Bi$ : Bernstein basis function

In this study, B-spline curve was used to design of the free-form surfaces. The control points used in the design of the curve were determined as radii of curvature R14, R18, and R22. The knot points were randomly selected to have a free-form surface. The curves were drawn using the MATLAB program based on the B-Spline functions. The knot points used in the creation of the curves are the same for all, and these values are t0 = 1, t1 = 3, t2 = 5, t3 = 7, t4 = 9, t5 = 11, t6 = 13. The control points used to create the B-Spline curves are given in Table 1. The solid models of the surfaces were designed using the SOLIDWORKS 2016 package program, and the B-Spline curve and solid model of the R14 sample is given in Figure 1.

Table 1: Control points of the designed B-Spline curves.

| Curve | Control Points | | | |
|---|---|---|---|---|
| **R14** | $B_0$(20,20) | $B_1$(25,30) | $B_2$(45,30) | $B_3$(70,20) |
| **R18** | $B_0$(24,24) | $B_1$(29,34) | $B_2$(49,34) | $B_3$(74,24) |
| **R22** | $B_0$(28,28) | $B_1$(33,38) | $B_2$(53,38) | $B_3$(78,28) |

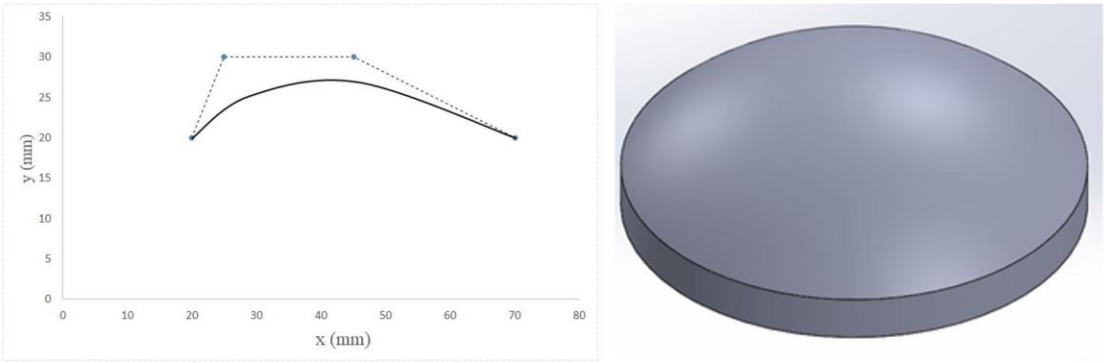


Figure 1: B-Spline Curve (a) and solid model of the R14 surface (b).

## 2.2 Production of Samples

Ti13Nb13Zr alloy conforming to ASTM F-1713 standard was commercially obtained from Baoji Titanium Future Company. A mold was designed in SolidWorks 2016 software to produce the free-form shaped samples. The mold was produced using AISI 1040 steel on the HAAS brand VF-3SS model 5-axis CNC machine in the workshop of Ottoman Group Implant Company. Ti13Nb13Zr alloy samples were prepared for production by hydraulic press, in a time and temperature-controlled heat treatment furnace, by rising to 200 °C in 10 minutes and keeping them at this temperature for 10 minutes. The samples were taken out from the furnace, and then pressed under 860 MPa pressure between the male and female molds placed in the hydraulic

press, and the free-form shaped samples were produced successfully without any undesired plastic deformation. Then, the sample surfaces were polished with polishing machine to prepare for the PVD coating processes. The mirror-like polished samples were washed in ultrapure water in an ultrasonic bath for 15 minutes, then prepared for the coating process and stored in vacuum bags.

### 2.3 Coating Procedure

Multilayer coatings were deposited using a DC-pulsed closed-field unbalanced magnetron system (Teer Coatings). The samples were subjected to an ion cleaning process using Argon gas at 2.66 Pa pressure, -800 Bias voltage for 30 minutes. A thin titanium adhesion layer was deposited to enhance the adhesion between the coatings and the substrate. Titanium nitride (TiN)/ titanium carbide (TiC) / titanium carbo-nitride (TiCN) thin films were deposited in the interlayers, repeating six times, and tantalum nitride (TaN) was deposited on the top layer. R14, R18 and R22 samples were coated with the same coating architecture (Figure 2). Pulsed DC parameters were 150 kHz frequency, and 2 μs period for all TiN, TiC, TiCN, and TaN coatings. Detailed coating parameters can be seen in Table 2.

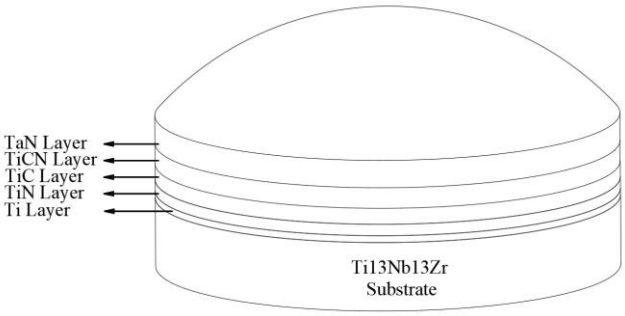


Figure 2: Coating Architecture.

Table 2: Coating Parameters.

| | Layer | | | | |
|---|---|---|---|---|---|
| **Parameter** | **Ti** | **TiN** | **TiC** | **TiCN** | **TaN** |
| Work Pressure (Pa) | 3.34 | 3.34 | 3.34 | 3.34 | 3.34 |
| Flow rate of $N_2$ (sccm) | - | 7 | - | 7 | 14 |
| Flow rate of Ar (sccm) | 7 | 7 | 7 | 7 | 7 |
| Bias Voltage (V) | -70 | -70 | -70 | -70 | -70 |
| Deposition Time (min.) | 10 | 8 | 8 | 8 | 70 |

### 2.4 Characterization Experiments

The wear resistance of thin-film coatings deposited on flat surfaces has traditionally been determined in pin-on-disc or ball-on-disc wear devices. Since the wear resistance of thin films deposited on samples with curved surfaces cannot be determined with these devices, purpose-built wear test setups are being developed. In this study, to determine the wear behavior of multilayer TiN/TiC/TiCN/TaN films deposited on the curved Ti13Nb13Zr alloy substrate, a wear test setup was developed on a lathe machine (Figure 3). Since the Ti13Nb13Zr alloy is a

biomaterial, wear tests were performed in simulated body fluid (SBF) environment. And an ultra-high molecular weight polyethylene (UHMWPE) material, whose surface was machined in the same curvature form as Ti13Nb13Zr alloy, was used as the counter component in the wear tests. Simulated body fluid was prepared according to Kokubo's recipe (Kokubo et al.,2006). Accordingly, to prepare one liter of SBF, the reagents in the Table 3 below were added to 700 ml of pure water in a glass bottle in the given amounts, respectively. More detailed information about the preparation of SBF can be found in Kokubo's article.

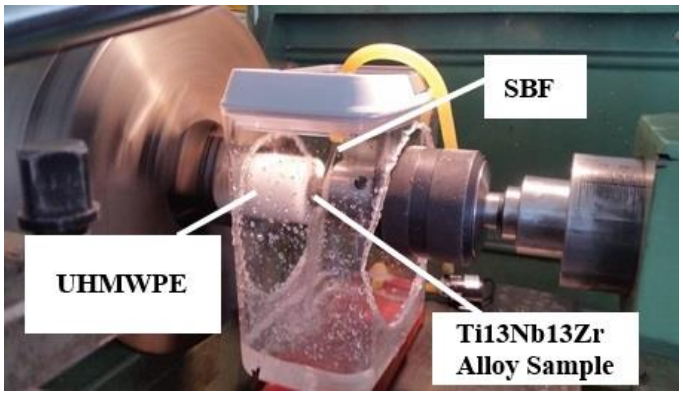

Figure 3: Wear experiment design.

Table 3: Reagents used to prepare 1L SBF.

| Order | Reagent | Amount |
|---|---|---|
| | NaCl | 8.035 g |
| 2 | $NaHCO_3$ | 0.355 g |
| 3 | KCl | 0.225 g |
| 4 | $K_2HPO_4 . 3H_2O$ | 0.231 g |
| 5 | $MgCl_2 . 6H_2O$ | 0.311 g |
| 6 | $1.0_M$-HCl | 39 ml |
| 7 | $CaCl_2$ | 0.292 g |
| 8 | $Na_2SO_4$ | 0.072 g |
| 9 | Tris | 6.118 g |
| 10 | $1.0_M$-HCl | 0-5 ml |

The UHMWPE component was connected to the chuck of the lathe, and the coated Ti13Nb13Zr sample was screwed to the traveling tailstock of the lathe by opening a screw thread on its back. A dynamometer was added to the system to control the applied force during the experiments. Before applying force, the wear components were reset by bringing them into contact with each other, then 800 N load was applied by controlling the forward movement of the tailstock. Chuck speed was set to 105 rpm during experiments, and the mass loss of the UHMWPE was determined by stopping the experiment every $10^6$ cycles, removing the UHMWPE component, and measuring the weight on a precision balance. In addition, the simulated body fluid was renewed every $10^6$ cycles, thus preventing the wear particles from causing more wear by acting as the third body. Since the standard minimum number of cycles required in the wear tests of orthopedic joint implants used in the biomedical field is $5x10^6$, the wear tests were performed in this total number

of cycles. The morphology of the deposited multilayer thin films was investigated using SEM. Tribological and adhesion properties of the multilayer thin films were examined with an optical microscope and SEM-EDS analysis. Image Focus software was used to calculate the failure amount of the coatings.

## 3.0 RESULTS AND DISCUSSION

Cross section SEM image of the multilayer thin films deposited on the R22 sample is given in Figure 4. The total thickness was measured at approximately 2.62 µm, and the coating layers can be seen clearly. It is understood that the deposited thin films do not show any discontinuity or irregularity in the image area. However, it is striking that there are different penetration depths in the region where the TaN layer is deposited on the TiCN layer.

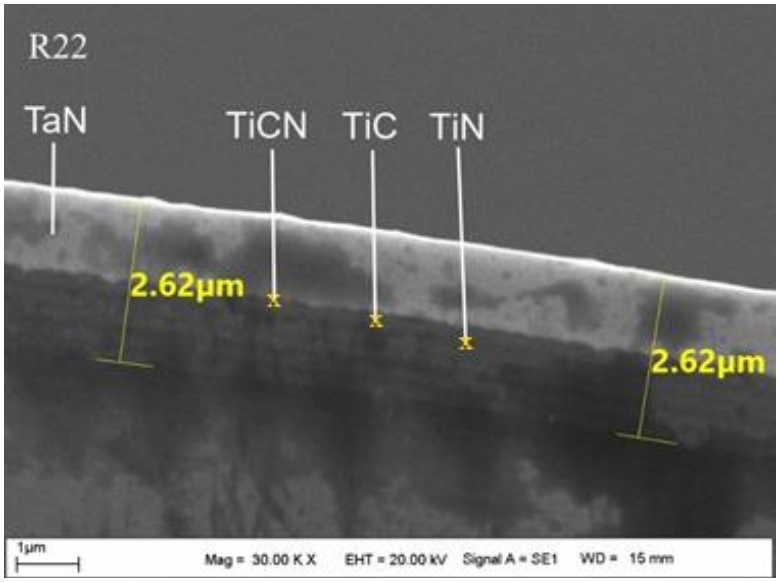


Figure 4: Cross section SEM images of the R22.

The mass losses in the UHMWPE component as a result of the wear experiments are given in Table 4. For the uncoated R14 and the coated R14, R18, and R22 samples, the interoperable ultra-high molecular weight polyethylene components were coded as P0, P14, P18, and P22, respectively. It was determined that there was a mass loss of 15.45 mg at the end of 5 million cycles in the UHMWPE component, which was subjected to the wear test with the uncoated sample. As a result of the wear test performed in 5 million cycles (mc) with the R14 sample, which has the same radius of curvature, the mass loss of the UHMWPE component was determined as 6.75 mg. This result shows that thanks to the TiN/TiC/TiCN/TaN multi-layer coating, the wear on the polyethylene component was reduced by 2.28 times. When the wear amounts of the samples are evaluated according to the radius of curvature, it is understood that the amount of wear in the UHMWPE component increases depending on the increasing radius of curvature.

Table 4: Wear amounts of UHMWPE samples.

| | Cycle | | | | |
|---|---|---|---|---|---|
| | $10^6$ | $2\times10^6$ | $3\times10^6$ | $4\times10^6$ | $5\times10^6$ |
| **Sample** | **Wear amount (mg)** | | | | |
| P0 | 1.25 | 3.45 | 6.28 | 10.52 | 15.45 |
| P14 | 1.12 | 2.25 | 4.65 | 5.68 | 6.75 |
| P18 | 1.21 | 2.34 | 4.89 | 5.95 | 8.15 |
| P22 | 1.18 | 2.58 | 5.12 | 7.23 | 12.34 |

UHMWPE is widely used in hip and knee implants as a load-bearing element in biomedical joint implants, often matching with a metal component. According to the in-vivo results of these applications and the data obtained from various in-vitro experimental studies, the average wear rate obtained in the jointing of the polyethylene component with CoCr or Titanium alloy counter material has been reported as 8 mg/mc (Cho et al., 2012; Ezzet et al., 2012; Abdel-Jaber et al., 2015). From this point of view, it can be said that TiN/TiC/TiCN/TaN multilayer coatings deposited on Ti13Nb13Zr alloy gave successful results since a 1.35 mg/mc wear rate was obtained in this study.

After the wear test, EDS-mapping investigations were carried out to understand which layers the coating failure occurred (Figure 5). According to the mapping investigations, it is understood that the light gray area layer on the left is the TaN layer where failure did not occur. In the region on the right, it is seen that there is densely Titanium, a small amount of carbon, and a lesser amount of nitrogen. Thus, it is understood that where the TaN layer is delaminated is the TiCN layer located just below the TaN layer in the coating architecture. As a result of the wear test of the R14 sample, which was applied in 5 million cycles, it was determined that only the uppermost, the TaN layer, was partially delaminated. Optical microscope and SEM images of the surface of the R14 sample after the wear experiment are given in Figure 6. It is seen that there are prominent abrasive wear lines at the top of the surface, the wear lines become blurred with the decrease of the slope, and the TaN layer is delaminated at regions near the edge. It is understood that the wear mechanism is completely abrasive in the upper parts of the surface, and the adhesive wear mechanism becomes dominant in the lower parts of the surface with the decrease of the slope. The failure of the TaN layer, which started in the regions close to the edge with the decrease of the slope, progressed in the form of a thin band with variable width and expanded up to a maximum of 2 mm from the edge. The total area of the delaminated TaN layer was calculated using the multi-point polygon method in the Image Focus software and was found to be 32.28 $mm^2$. When this value is compared to the total surface area of the coating, which is 369.63 $mm^2$, it was found that the layer damage occurred in 8.73% of the coating. Besides, the adhesion areas of the UHMWPE wear particles and the regions where fretting corrosion occurs on the sample surface are seen in the SEM image. Fretting corrosion is a type of corrosion that occurs as a result of the cycle loading damage to the oxide films on the surfaces of metal alloys working in contact with each other (Diomidis, 2012). Although UHMWPE is the reciprocating material in this study, it is understood that fretting corrosion occurs due to instantaneous damage to the self-forming $Ta_2O_5$ oxide layer on the surface of the multilayer-coated metal alloy. The fact that the simulated body fluid used in the experiment has a very aggressive structure in terms of corrosion is also thought to be effective in the occurrence of this type of wear.

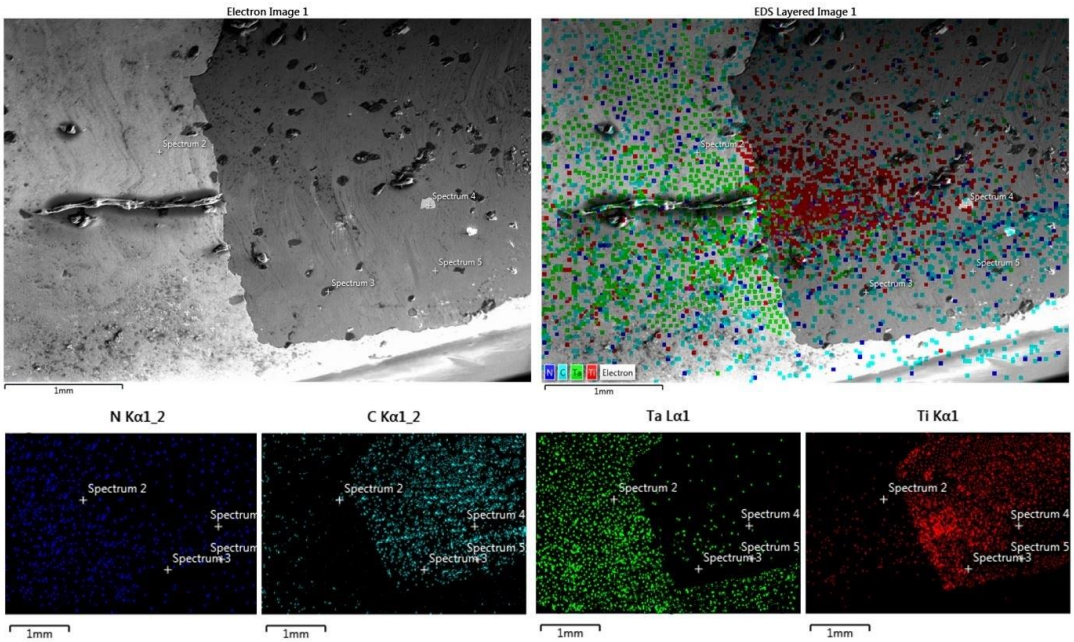


Figure 5: EDS elemental mapping of the surface of the R14 sample after the wear test.

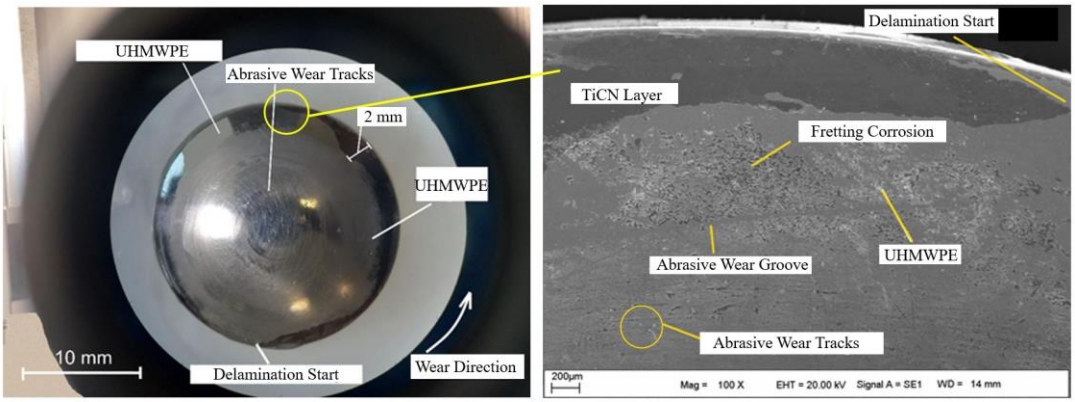


Figure 6: Optical microscope and SEM images of the R14 sample.

EDS elemental mapping of the worn surface of the R18 sample is given in Figure 7. The presence of intense Titanium in the dark region, the concentration of carbon, and the small amount of nitrogen content indicate that this region is the TiCN layer under the TaN layer. This result indicates that only the TaN layer has been exposed to failure after the wear test. When the optical and SEM images of the R18 sample were studied, the presence of abrasive wear lines parallel to the wear direction on the surface, which gradually decreases from the apex to the bottom, shows that the wear in this sample is mostly of abrasive character too (Figure 8). The failure of the TaN layer first started as a thin band, then continued to expand, extended to a maximum distance of 2.75 mm from the edge, and then ended as a wide band. It is understood from the presence of abrasive pick-up grooves and lines that abrasive wear is dominant as it

moves away from the edge. The failure area in the TaN layer was measured as 43.29 mm$^2$, which corresponds to approximately 12.6 % of the total surface area of the coating. Fretting corrosion zones and wear particles of the ultra-high density polyethylene component adhered to the surface are seen for this coating too.

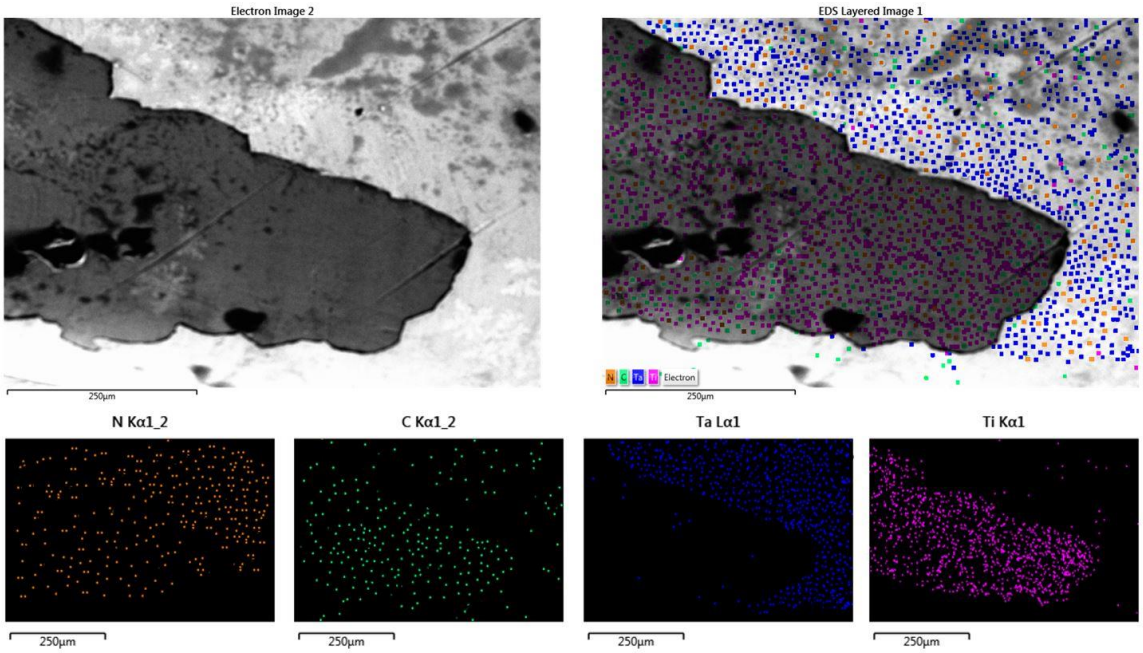


Figure 7: EDS elemental mapping of the surface of the R18 sample after the wear test.

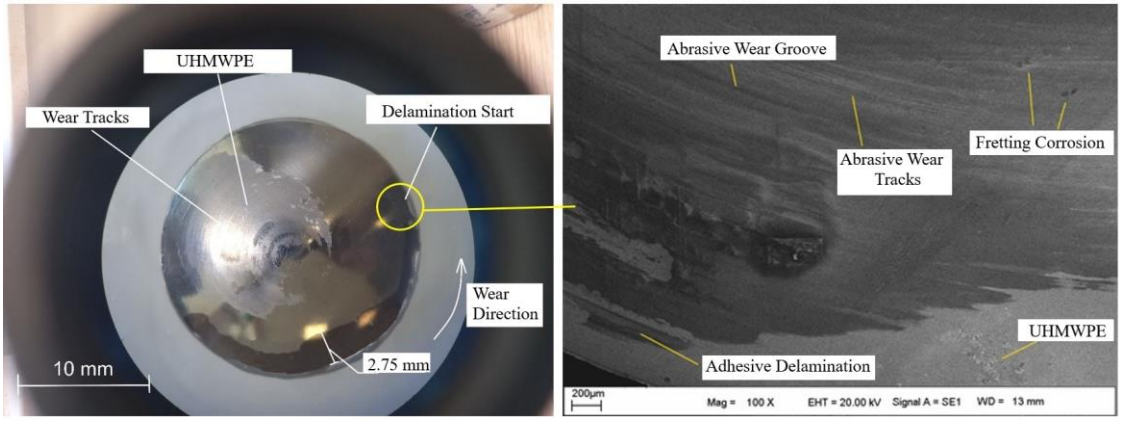


Figure 8: Optical microscope and SEM images of the R18 sample.

As a result of the wear test of the coating on the sample surface with a radius of curvature of R22, it is understood from Figure 9 that, unlike the others, not only the TaN layer is delaminated, but also the TiCN and TiC layers are delaminated too. It can be seen clearly from the elemental distribution analysis that the relatively darker gray region is the TiCN layer, and the black is the

TiC layer. It is understood that the failure of the coating showed discontinuities and occurred in different regions (Figure 10). In the first failure zone, layer deformation started at a point, then progressed from the edge inwards in the form of dendritic indentations and ended at a point. A secondary deformation zone extends inward from the edge in a dendritic form but continues to expand in a continuous and stable structure after a specific region. The maximum distance of the coating failure from the edge was measured to be approximately 3 mm and is more than the maximum failure amount on the other two free-form coating surfaces. The failure amount in the coating layer on this sample surface was measured as 56.15 mm$^2$, which corresponds to 16.89 % of the total sample surface area. This indicates that coating failure is twice as compared to the sample with the R14 radius of curvature. Along with the presence of fretting corrosion areas on the coating surface and the surfaces where the coating has been delaminated, the presence of abrasive wear particles can also be observed. It can be seen from the images that adhesive and abrasive wear occurred together on this sample surface, but adhesive wear is more dominant.

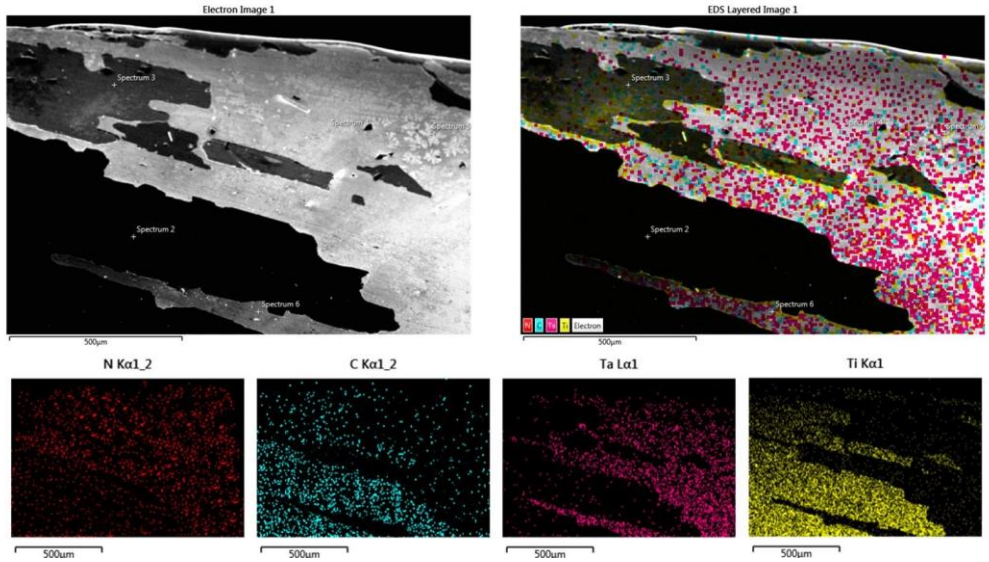


Figure 9. EDS elemental mapping of the surface of the R22 sample after the wear test.

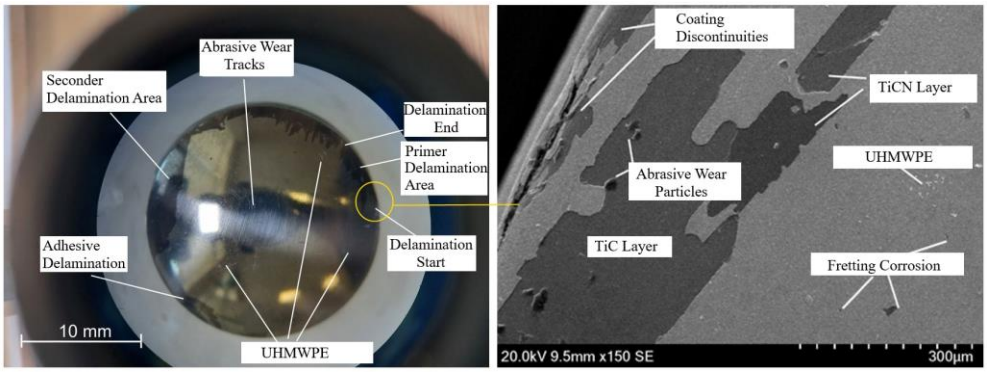


Figure 10: Optical microscope and SEM images of the R18 sample.

It was observed that adhesive failures occurred at the edges and near the edges of all samples with different radii of curvature. Similarly, it was determined that abrasive wear occurred at the peaks of all samples. Adhesive failure of thin film coatings is due to poor adhesion with the substrate material surface (Holmberg et al., 2009). However, in this study, adhesive failure of only the TaN layer (coatings on R14 and R18 sample), not all coating layers, indicates a weak adhesion between this layer and the TiCN layer located just below it.

In the PVD-Magnetron sputtering coating technique, samples are placed on the holder as their surfaces face the targets (Figure 11). The high-purity target material, which is the thin film component to be deposited on the surface, is subjected to ionic bombardment with reactive Argon gas, thus scattering the target material ions (Kern et al., 2002). These scattered ions turn into a dense plasma on the sample holder located in the center of the room, thanks to the closed unbalanced electromagnetic field. Meanwhile, the positively charged target material ions in the plasma are deposited on the negatively charged substrate material surface. Parameters such as the distance between the target material and the substrate placed on the sample holder and the rotation speed of the sample holder directly affect the morphology of the deposited thin films, as they determine the level of plasma utilization of the substrate material. Therefore, during the thin film deposition on flat surfaces, the entire surface can benefit from plasma effectively due to the equal distance between the target and the substrate material (Ohring, 2002). In this study, although the surfaces to be coated were placed on the same sample holder facing the target materials, the top surface of the substrate materials was closer to the target material, and the edge areas were farther away due to the surface curvature. As a result, a more homogeneous and stable film was deposited on the upper parts of the surfaces compared to the edges. Since the distance of the edge regions to the plasma increased due to the increase in the radius of curvature of the samples, the coating with the weakest adhesion and lowest tribological properties was obtained in the R22 sample. Previous studies have reported that thin films deposited on different substrate materials with variable methods have varying thickness and morphology depending on the surface curvature, so it has been understood that the results obtained are compatible with the literature data (Kvasnicka et al., 1999; Liu et al., 2013; Hirata et al., 2015).

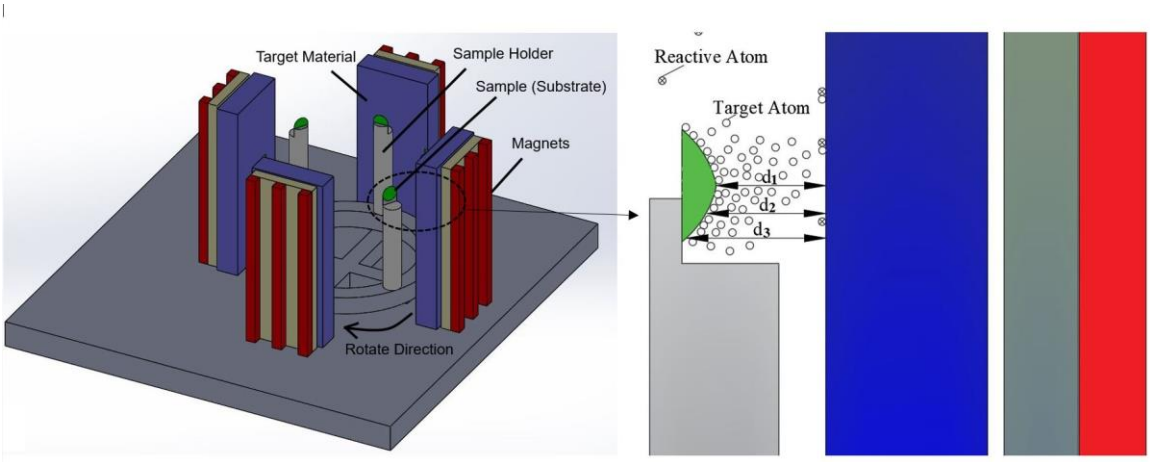


Figure 11: Schematic representation of PVD magnetron sputtering process.

## CONCLUSIONS

The surfaces designed with the Bezier curve method were successfully manufactured and were multilayer coated via the unbalanced magnetron sputtering method. As a result of the wear test in which UHMWPE was used as the counter material, it was determined that the multilayer coated sample increased the wear resistance of the UHMWPE component by 2.28 times. Additionally, it was understood that the mass loss in the UHMWPE component increased as the radius of curvature of the surface-coated samples increased.

As a result of the worn surface examination of the coated Ti13Nb13Zr alloy samples, it was observed that abrasive wear occurred at the top region of all samples, and adhesive wear occurred in the areas close to the edges. This finding can be interpreted as the morphological properties of thin films deposited on curved surfaces in the magnetron sputtering process are not homogeneous on all surfaces. This result was thought to be obtained because the distance of the samples with curvilinear surfaces to the target material varies depending on the surface slope. As a result of the wear test, the fact that the least failure occurred in the thin films deposited on the sample surface with the smallest curvature radius and the highest amount of failure occurred in the R22 sample with the high curvature radius confirms this perspective. It was determined by SEM-EDS elemental mapping examination that only the TaN layer was delaminated in the wear test in the R14 and R18 coatings, and unlike them, the TiCN layer was also delaminated in the R22 sample. Based on this, it can be claimed that the TaN layer shows weak adhesion on the TiCN layer. Although the wear rates obtained in this study are acceptable for the UHMWPE component, they cannot be considered within acceptable limits due to delamination occurring in the coating layers, especially the TaN layer, on the Ti13Nb13Zr alloy surface. To deposit thin films with a more homogeneous structure on free-form surfaces, it is recommended as a future study to define a movement in the sample holder by the surface curvature so that all surfaces of the sample can effectively benefit from plasma during the coating process.

## ACKNOWLEDGMENTS

This scientific research has been financially supported by the Scientific Research Project Committee of İnonu University (No: FDK 2020-2089) and Ottoman Group Implant CO. The authors are grateful for this support.

## REFERENCES

Abdel-Jaber S., Belvedere C., Leardini A., & Affatato S. (2015). Wear simulation of total knee prostheses using load and kinematics wave forms from stair climbing. Journal of Biomechanics, 48 (14), 3830-3836.

Abdi F., & Savaloni H. (2015). Investigation of the growth conditions on the nanostructure and electrical properties of ZnS chiral sculptured thin films. Applied Surface Science, 330, 74–84

Ayhan E. (2003). "Kanca Yüzeyi Geometrsinin Sentetik Eğriler ile Modellenmesi ve Optimizasyon" (Master's thesis). The council of Turkey Higher Education National Thesis Center Database (UMI No. 142771).

Bahçe E., & Özdemir B. (2020). Analyzing the effects of different tool paths on form errors in the milling of freeform surfaces. Sigma Journal of Engineering and Natural Sciences, 38 (3), 1321-1332.

Birkett M., Zia A.W., Devarajan D.K., Soni., Panayioditis M. I., Joyce T. J., Tambuwala M. M., & Serrano-Aroca A. (2023). Multi-functional bioactive silver- and copper-doped diamond-like carbon coatings for medical implants. Acta Biomaterialia, 167, 54-68.

Byoung K.C. & Jerard R.B. (1998). Sculptured Surface Machining. USA: Springer

Cho C., Murakami T., & Sawae Y. (2012). Wear phenomena of ultra-high molecular weight polyethylene (UHMWPE) joints. In Affatato S. (eds.), Wear of orthopaedic implants and artificial joints, (pp.221-245). UK: Woodhead Publishing Limited.

Diomidis N. (2012). Wear phenomena of metal joints. In Affatato S. (eds.), Wear of orthopaedic implants and artificial joints, (pp.221-245). UK: Woodhead Publishing Limited.

Esfendiar A., Savaloni H., & Placido F. (2013). On the fabrication and characterization of graded slanted chiral nano-sculptured silver thin films. Physica E, 50, 88–96.

Ezzet K.A., Hermida J.C., Steklov N., & D'Lima D.D. (2012). Wear of Polyethylene Against Oxidized Zirconium Femoral Components Effect of Aggressive Kinematic Conditions and Malalignment in Total Knee Arthroplasty. The Journal of Arthroplasty, 27(1), 116-121.

Gao Z., Zhang T., Wang Q. & MayrhoferP.H. (2023). Nanostructured zig-zag γ-Mo2N thin films produced by glancing angle deposition for flexible symmetrical solid-state supercapacitors. Materials&Design, 225, 11432.

Gomes C.C., Moreira L.M., Santos V.J.S.V., Ramos A.S., Lyon J.P., Soares C.P., & Santos F.V. (2011). Assessment of the genetic risks of a metallic alloy used in medical implants. Genetics and Molecular Biology, 34(1), 116-121.

Gong L., Fan C., Shen Z., Chen Z. & Zhang Lei. (2023). Research on discretization algorithm of free-form surface for robotic polishing. Journal of Manufacturing Processes, 92, 350-370.

Grineviciute L., Buzelis R., Mazule L., Melninkaitis A., Kičas S., & Tolenis T. (2020). Enhancement of high reflectivity mirrors using the combination of standard and sculptured thin films. Optics and Laser Technology, 129, 106292.

Herbster M., Döring J., Nohava J., Lohmann C.H., Halle T., & Bertrand J. (2020). Retrieval study of commercially available knee implant coatings TiN, TiNbN and ZrN on TiAl6V4 and CoCr28Mo6. Journal of the Mechanical Behavior of Biomedical Materials, 112, 104034.

Hirata Y., Kato T., & Choi J. (2015). DLC coating on a trench-shaped target by bipolar PBII, Int. Journal of Refractory Metals and Hard Materials. 49, 392-399.

Holmberg K., & Matthews A. (2009). Coatings Tribology, UK: Elsevier.

Hussein M., Kumar M., Ankah N. & Abdelaal A. (2023). Surface, mechanical, and in vitro corrosion properties of arc-deposited TiAlN ceramic coating on biomedical Ti6Al4V alloy. Trans. Nonferrous Met. Soc. China, 33, 494−506.

Ibrahim S.W. & Hamad T.I. (2023). Electrospun nano-barium Titanate/polycaprolactone composite coatings on titanium and Ti13Nb13Zr alloy. Composites and Advanced Materials, 32, 1–17.

Jiang X.J. & Scott P.J. (2020). Advanced Metrology-Free Form Surfaces. UK: Elsevier.

Kaur M., & Singh K. (2019). Review on titanium and titanium-based alloys as biomaterials for orthopaedic applications. Materials Science & Engineering C, 102, 844–862.

Kazek-Kesik A., Dercz G., Suchanek K., Kalemba-Rec I., Piotrowski J., & Simka W. (2015). Biofunctionalization of Ti–13Nb–13Zr alloy surface by plasma electrolytic oxidation. Part I. Surface & Coatings Technology, 276, 59–69.

Kazek-Kesik A., Krok-Borkowicz M., Dercz G., Donesz-Sikorska A., Pamula E., & Simka W. (2016). Multilayer coatings formed on titanium alloy surfaces by plasma electrolytic oxidation-electrophoretic deposition methods. Electrochimica Acta, 204, 294-306.

Kern W. & Schuegraf K. (2002). Deposition Technologies and Applications: Introduction and Overview. In Seshan K. (eds.), Handbook Of Thin-Film Deposition Processes And Techniques: Principles, Methods, Equipment and Applications (pp. 11-44). Norwich: Noyes Publications.

Kokubo T. & Takadama H. (2006). How useful is SBF in predicting in vivo bone bioactivity? Biomaterials, 27, 2907-2915.

Kopova I., Kronek J., Bacakova L., & Fencl J. (2019). A cytotoxicity and wear analysis of trapeziometacarpal total joint replacement implant consisting of DLC-coated Co-Cr-Mo alloy with the use of titanium gradient interlayer. Diamond and Related Materials, 97, 107456.

Kumar M., Kumar R., & Kumar S. (2021). Coatings on orthopedic implants to overcome present problems and challenges: A focused review. Materials Today: Proceedings, 45, 5269–5276.

Kvasnicka I., Mala Z., Novak R., & Novakova D. (1999). Effect of substrate curvature on the properties of PVD coatings. Surface and Coatings Technology, 116–119 , 634-637.

Li Y., Yang C., Zhao H., Qu S., Li X., & Li Y. (2014). New Developments of Ti-Based Alloys for Biomedical Applications. Materials, 7, 1709-1800.

Liu D., Seraffon M., Flewitt P.E.J., Simms N.J., Nicholls J.R., & Rickerby D.S. (2013). Effect of substrate curvature on residual stresses and failure modes of an air plasma sprayed thermal barrier coating system. Journal of the European Ceramic Society, 33, 3345-3357.

Lopes C., Rodrigues M.C., Ferreirea A., Macedo F., Borsan I., Gabor C. et al. (2023). The influence of the nanostructure design on the optical, electrical and thermal properties of TiNx thin films prepared by reactive magnetron sputtering. Materials Chemistry and Physics,306,127981.

Lützner, J., Hartmann, A., & Dinnebier, G. et al. (2013). Metal hypersensitivity and metal ion levels in patients with coated or uncoated total knee arthroplasty: a randomized controlled study. International Orthopaedics (SICOT), 37, 1925–1931.

Martín-Palma R.J. & Lakhtakia A. (2013). Oblique-angle deposition: evolution from sculptured thin films to bioreplication. Scripta Materialia, 74, 9-12.

Miura K. T., & Ru G. (2014). Aesthetic curves and surfaces in computer aided geometric design. International Journal of Automation Technology, 8(3), 304-316.

Ohring M. (2002). Thin-Film Evaporation Processes. In Ohring M. (eds.), Materials Science of Thin Films Deposition and Structure (pp.95-144). USA: Academic Press.

Ossowska A., Sobieszczyk S., Supernak M., & Zielinski A. (2014). Morphology and properties of nanotubular oxide layer on the "Ti–13Zr–13Nb" alloy. Surface & Coatings Technology, 258, 1239-1248.

Özdemir B. (2015). "Serbest şekilli yüzeylerin işlenmesinde işleme parametrelerinin form hatalarına etkilerinin incelenmesi" (Master's thesis). The council of Turkey Higher Education National Thesis Center Database (UMI No. 390636).

Pawłowski Ł., Mania S., Banach-Kopec A., Bartmanski M., Ronowska A., Jurak K., et al. (2023). Osteoblast and bacterial cell response on RGD peptide-functionalized chitosan coatings electrophoretically deposited from different suspensions on Ti13Nb13Zr alloy, J Biomed Mater Res. ;111:1800–1812.

Piotrowska K. & Madej M. (2023). Tribological Properties of Silver Doped Titanium Nitride Coatings. Tribologia, 3, 43-51.

Pourzadeh D. & Savaloni H. (2023). Design and fabrication of Cu conical (Spiral+Helical) sculptured thin films and their application in SERS. Optical Materials, 146, 114430.

Pu J., Zhang Y., Zhang X., Yuan X., Yang S., Zhang G., Cui W., Tan Q. & Jin Z. (2023). Fretting corrosion behavior of Ti6Al4V alloy against zirconia-toughened alumina ceramic in simulated body fluid. Journal of the Mechanical Behavior of Biomedical Materials, 142, 105860.

Rafiq N.M., Wang W., Liew S.L., Chua C.S., & Wang S. (2023). A review on multifunctional bioceramic coatings in hip implants for osteointegration enhancement. Applied Surface Science Advances, 13, 100353.

Rahchamani S.Z., Dizaji H.R.G., & Ehsani M.H. (2015). Fabrication of ZnS Zigzag Sculptured Nanostructured Thin Films. Procedia Materials Science, 11, 464 – 468.

Reyna A.L.P., Fritz B., Schwiesau J., Schilling C., Summer B., Thomas P., & Grupp T.M. (2018). Metal ion release barrier function and biotribological evaluation of a zirconium nitride multilayer coated knee implant under highly demanding activities wear simulation. Journal of Biomechanics, (79), 88-96.

Robbie K. & Brett M.J. (1997). Sculptured thin films and glancing angle deposition: Growth mechanics and applications. Journal of Vacuum Science & Technology A, 15, 1460–1465.

Rothammer B., Neusser K., Bartz M., Wartzack S., Schubert A., & Marian M. (2023). Evaluation of the wear-resistance of DLC-coated hard-on-soft pairings for biomedical applications. Wear, 523, 204728.

Savaloni H., Fakharpour M., Siabi-Garjan A., Placido F., & Babaei F. (2017). Nano-structure and optical properties (plasmonic) of graded helical square tower-like (terraced) Mn sculptured thin films. Applied Surface Science, 393, 234–255.

Savari R., Savaloni H., Abbasi S., & Placido F. (2018). Design and engineering of ionization gas sensor based on Mn nano-flower sculptured thin film as cathode and a stainless steel ball as anode. Sensors and Actuators B Chemical, 266, 620-636.

Schmidt D., Müller C., Hoffman T., Inganas O., Arwin H., Schubert E., & Schubert M. (2011). Optical properties of hybrid titanium chevron sculptured thin films coated with a semiconducting polymer. Thin Solid Films, 519, 2645–2649.

Schroeder S., Braun S., Mueller U., Schroeder M., Sonntag R., Jaeger S., & Kretzer J.P. (2020). Polyethylene wear and metal release of TiNbN-coated knee implants. Wear, 458-459, 203426.

Senopati G., Rahman Rashid R.A., Kartika I. & Palanisamy S. (2023). Recent Development of Low Cost β-Ti Alloys for Biomedical Applications: A Review, Metals, 13, 194.

Skjöldebrand C., Tipper J.L., Hatto P., Bryant M., Hall R.M., & Persson C. (2022). Current status and future potential of wear-resistant coatings and articulating surfaces for hip and knee implants. Materials Today Bio, 15, 100270.

Soltane H.B., Akkari F.C., Gallas B. & Kanzari M. (2023). Structural, morphological, and optical properties of AgxO thin films deposited via obliquely angle deposition. Materials Science Poland, 41 (1), 27-41.

Sowa M., Piotrowska M., Widziolek M., Dercz G., Tylko G., Gorewoda T., Osyczka A.M., & Simka W. (2015). Bioactivity of coatings formed on Ti–13Nb–13Zr alloy using plasma electrolytic oxidation. Materials Science and Engineering C, 49, 159-173.

Stroz A., Losiewicz B., Zubko M., Chmiela B., Balin K., Dercz G., Gawlikowski M., & Goryczka T. (2017). Production, structure and biocompatible properties of oxide nanotubes on Ti13Nb13Zr alloy for medical applications. Materials Characterization, 132, 363-372.

Urbanczyk E., Krzakala A., Kazek-Kesik A., Michalska J., Stolarczyk A., Dercz G., & Simka W. (2016). Electrochemical modification of Ti–13Nb–13Zr alloy surface in phosphate-based solutions. Surface & Coatings Technology, 291, 79-88.

Ye J., Chen L., Li X., Yuan Q., & Gao Z. (2017). Review of optical freeform surface representation technique and its application. Optical Engineering, 56 (11), 110901.

Zhang L.C. & Chen L.Y. (2019). A Review on Biomedical Titanium Alloys: Recent Progress and Prospect. Advanced Engineering Materials. 1801215.

Zhang Y., Xiu P., Jia Z., Zhang T., Yin C., Cheng Y., Cai H., Zhang K., Song C., Leng H., Yuan W., & Liu Z. (2018). Effect of vanadium released from micro-arc oxidized porous Ti6Al4V on biocompatibility in orthopedic applications. Colloids and Surfaces B: Biointerfaces, 169, 366-374.